NASA TECHNICAL NOTE

NASA TN D-5966

NASA MINITRACK INTERFEROMETER REFRACTION CORRECTIONS

by P. E. Schmid

Goddard Space Flight Center
Greenbelt, Md. 20771

NATIONAL AERONAUTICS AND SPACE ADMINISTRATION • WASHINGTON, D. C. • MARCH 1971

1. Report No.	2. Government Accession No.	3. Recipient's Catalog No.
NASA TN D-5966		

4. Title and Subtitle	5. Report Date
NASA Minitrack Interferometer Refraction Corrections	March 1971
	6. Performing Organization Code
7. Author(s) P. E. Schmid	8. Performing Organization Report No. G-974
9. Performing Organization Name and Address	10. Work Unit No.
Goddard Space Flight Center Greenbelt, Maryland 20771	11. Contract or Grant No.
	13. Type of Report and Period Covered
12. Sponsoring Agency Name and Address	Technical Note
National Aeronautics and Space Administration Washington, D.C. 20546	14. Sponsoring Agency Code

15. Supplementary Notes

This report is a republication of NASA-GSFC Document X-551-69-434, October 1969.

16. Abstract

The NASA Minitrack interferometer system is an accurate, reliable, and proven spacecraft tracking system. This report reviews the influence of the earth's atmosphere upon Minitrack calibration and spacecraft tracking. It is believed that this review will aid the orbit computation engineer in selecting those refraction correction procedures that will insure maximum orbit computation accuracy whenever an interferometer such as the Minitrack system is used.

17. Key Words Suggested by Author	18. Distribution Statement
Interferometer Atmospheric Refraction	Unclassified—Unlimited

19. Security Classif. (of this report)	20. Security Classif. (of this page)	21. No. of Pages	22. Price*
Unclassified	Unclassified	33	$3.00

*For sale by the National Technical Information Service, Springfield, Virginia 22151

SUMMARY

This report examines the refraction effects of the earth's atmosphere on the NASA 136-MHz Minitrack interferometer during aircraft calibration and spacecraft tracking. It is shown that only the troposphere (sea level to 30 km) affects aircraft calibration. It is also seen that the ionosphere (85 km to 1000 km) is the principal refraction bias source during spacecraft track. This results from the troposphere correction inherent in an interferometer angle calculation.

The bias induced by the daytime ionosphere at 25° elevation can be as large as 1 mrad. This bias decreases to 0.1 mrad at 80° elevation. During nighttime, when total ionosphere electron content decreases, refraction generally drops to only 10% of the daytime bias. Possible exceptions have been cited for near-equatorial stations where anomalous ionospheric behavior during nighttime has caused signal dropouts of Minitrack telemetry and tracking data. When present, this anomaly has been noted generally to peak at local midnight. If daytime data below elevation angles of 45° are to be used for precision orbit computation, it is clear that ionospheric refraction corrections are a necessary part of Minitrack data processing. These corrections are necessary to reduce the ionospheric refraction bias to a value comparable to the Minitrack system resolution of 0.1 mrad.

CONTENTS

NASA MINITRACK INTERFEROMETER REFRACTION CORRECTIONS*

by
P. E. Schmid
Goddard Space Flight Center

1.0 INTRODUCTION

This report reviews the influence of the earth's atmosphere upon NASA Minitrack measurements during system calibration and spacecraft tracking. The need for such a review stems from the increased number of precision orbits now being based upon Minitrack data (e.g., Reference 1), coupled with a lack of formal documentation in the area of Minitrack refraction modeling. The basic considerations presented in this report apply equally well to any short baseline radio interferometer tracking system.

Section 2.0 of this report briefly compares the angle information provided by an interferometer such as Minitrack with that obtained from steerable antenna systems. NASA steerable, or monopulse, tracking systems include—

(1) The GSFC Range and Range Rate system (Reference 2).
(2) The Unified S-Band system (Reference 3).
(3) The Pulse C-Band radar (Reference 4).
(4) The Applications Technology Satellite (ATS) Range and Range Rate system (Reference 5).

The earth's atmosphere can, for purposes of radiowave propagation analysis, be considered to consist of three layers. These layers, as indicated by Figure 1, are the troposphere (0 to 30 km), the free-space region (30 to 85 km), and the ionosphere (85 to 1000 km). Section 3.0 presents a brief description of the frequency independent tropospheric angle correction equations appropriate to steerable antenna spacecraft tracking. Section 4.0 indicates why the interferometer, to a first order, inherently corrects for tropospheric refraction when the baseline length is measured in free-space wavelengths at the spacecraft transmitter frequency. In section 5.0, it is pointed out that the effect of the one-way aircraft Doppler shift upon Minitrack calibration is negligible. For high-accuracy orbits, spacecraft Doppler effects (i.e., no effect at zenith, approximately 0.05-mrad maximum at $E = 30°$) should be modeled, and easily can be, in the orbit computation program.

Section 5.0 of this report reviews the philosophy of the present Minitrack aircraft calibration procedure, indicating the significance of radio and optical refraction. Equations are derived that

*This report is a republication of NASA-GSFC Document X-551-69-434, October 1969.

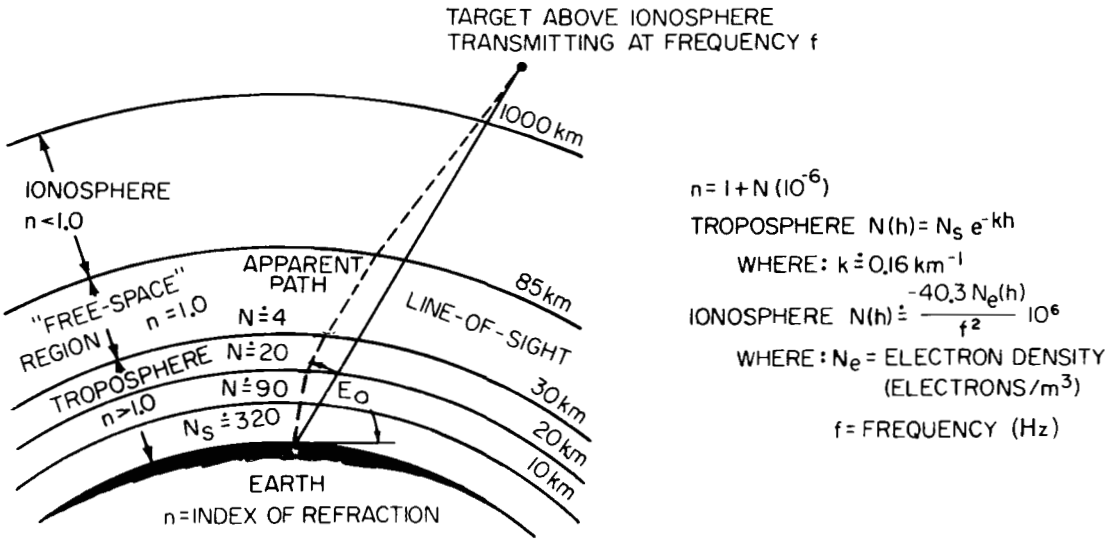

Figure 1—Relationship between troposphere and ionosphere.

properly model the atmosphere for purposes of calibration computations. These particular equations are incorporated in the Minitrack star background photoplate-reduction computer program used by the Physical Science Laboratory, New Mexico State University, for the GSFC.

Finally, section 6.0 indicates what improvements can be anticipated by modeling the ionosphere. Ray bending decreases in the ionosphere in proportion to the square of the transmission frequency (Reference 6). Thus, with an interferometer operating at S-Band frequencies (nominally 2 GHz), the distortion introduced by the ionosphere is reduced by a factor of approximately 200 relative to that at 136 MHz. By contrast, the tropospheric bending is independent of the frequency in the range of 100 MHz to 20 GHz (Reference 7).

Figure 2 indicates the overall Minitrack data handling and aircraft calibration interface. With regard to Figure 2, this report is primarily concerned with the optical and radio refraction corrections applied to the aircraft calibration data and with the inherent tropospheric corrections associated with data delivered to the orbit computation user and ionospheric refraction during spacecraft tracking.

Currently, aircraft calibration flights are performed approximately twice per year for each of the NASA Minitrack stations. (Site locations are presented in Figure 3.) The Minitrack and the GSFC Range and Range Rate systems are the primary tracking systems associated with the NASA Satellite Tracking and Data Acquisition Network (STADAN).

It should be mentioned that the primary purpose of the aircraft calibration is to determine the far-field phase characteristics of the Minitrack antenna array. The possibility of obtaining the same information via analysis of residuals from actual Minitrack satellite orbit calculations is currently under investigation.* A regression analysis of this type appears feasible if multiple station, short arc passes

*Oosterhout, J.D., Code 514 GSFC, "Minitrack Calibration," memorandum to C.H. Looney, Jr., Code 540 GSFC, August 19, 1968.

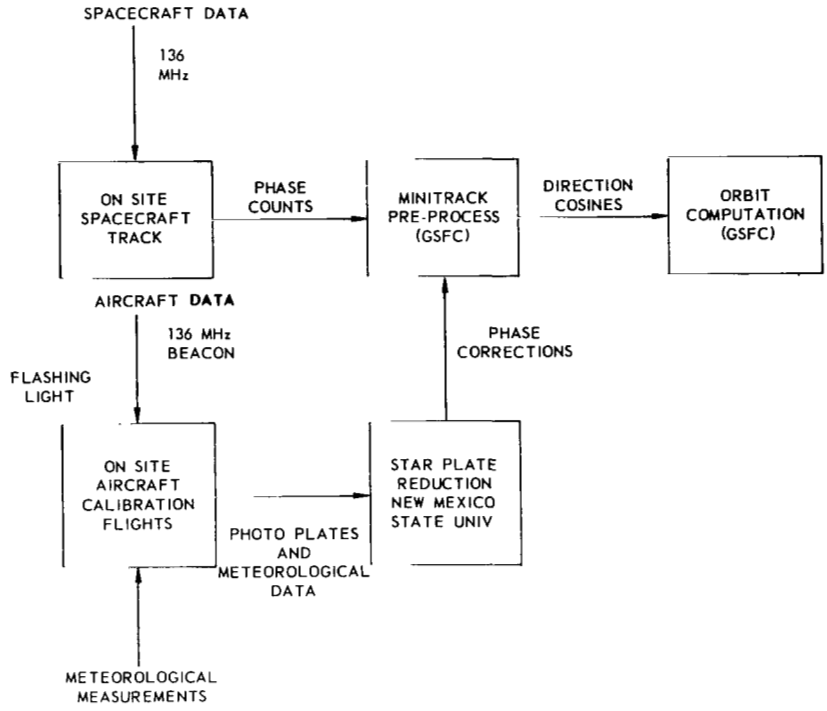

Figure 2—Overall Minitrack data handling.

Station	Present Status		Latitude			Longitude			Geodetic Height
	Active	Inactive or Closed	(deg	min	sec)	(deg	min	sec)	(meters)
Fairbanks, Alaska		X	64	52	18.61	212	09	40.15	189
Goldstone Lake, California		X	35	19	48.56	243	06	00.85	921
East Grand Forks, Minnesota		X	48	01	21.18	262	59	21.05	249
Fort Myers, Florida	X		26	32	53.78	278	08	04.60	9
Blossom Point, Maryland		X	38	25	49.91	282	54	49.37	6
St. John's, Newfoundland		X	47	44	28.94	307	16	46.71	112
Quito, Ecuador	X		-00	37	20.55	281	25	15.62	3578
Lima, Peru		X	-11	46	34.86	282	50	59.14	34
Antofagasta, Chile		X	-23	37	14.07	289	43	38.32	516
Santiago, Chile	X		-33	08	56.23	289	19	52.88	681
Winkfield, England	X		51	26	45.43	359	18	13.57	87
Johannesburg, South Africa	X		-25	53	00.98	27	42	28.49	1565
Tananarive, Madagascar	X		-19	00	25.21	47	18	00.46	1361
Woomera, Australia		X	-31	23	30.07	136	52	11.06	154
Orroral, Australia	X		-35	37	37.51	148	57	10.71	947
Gilmore Creek, Alaska	X		64	58	36.000	212	28	40.898	286

Figure 3—Satellite Tracking and Data Acquisition Network (STADAN) Minitrack stations.*

*Goddard Directory of Tracking Station Locations, NASA-GSFC Document X-554-67-54 as updated through November 1968.

are considered. Uncertainties in the earth geopotential function tend to mask tracking system biases when more than one earth revolution is calculated (Reference 8).

2.0 INTERFEROMETER VERSUS STEERABLE ANTENNA ANGLE MEASUREMENT

The Minitrack system is an interferometer tracking scheme (References 9 and 10) that provides angular data in the form of direction cosines describing the position of a spacecraft relative to a given tracking station. It is a passive system in which the spacecraft transmits at a nominal 136 MHz. Hence no ranging information is available, and at present no attempt is made to utilize the available, one-way Doppler frequency information for range rate calculations. The relationships between direction cosines and the conventional definitions of azimuth and elevation are given in Figure 4. As will be shown, the Minitrack direction cosine calculation does not provide a measure of either signal elevation angle of arrival or line-of-sight elevation to spacecraft but rather an elevation angle between the two, which, to a first order, is the angle of arrival corrected for tropospheric refraction. Elevation angle of arrival is the elevation angle of the incoming, essentially planar wavefront. Line-of-sight elevation is with reference to the straight line segment joining the interferometer array center and the spacecraft.

This is in contrast to the elevation angle-of-arrival measure provided by tracking systems employing steerable antennas (e.g., the NASA Unified S-Band, GSFC Range and Range Rate, and Pulse C-Band radar systems). The elevation angle of arrival is of course available directly from an azimuth-elevation antenna mount. It can be obtained by way of straightforward coordinate transformations when the angle data are measured with XY or polar antenna mounts (Reference 11).

3.0 TROPOSPHERIC ANGLE CORRECTION APPLIED TO STEERABLE ANTENNA TRACKING SYSTEMS

The usual correction scheme applied to elevation angle data obtained from tracking systems employing steerable antennas is

$$E = E_o - \Delta E = E_o - \Delta E_t - \Delta E_i \,, \tag{1}$$

where

E_o is the observed elevation angle of arrival,

ΔE is a correction accounting for atmospheric bending,

ΔE_t is associated with tropospheric bending,

and

ΔE_i is associated with ionospheric bending.

It should be pointed out that the effect of the ionosphere's presence is always to increase the error angle ΔE above that due to the troposphere alone. Since the bending within the ionosphere above the height of maximum ionization (h $\doteq$ 300 km) is in a direction opposite to that within the troposphere, one might assume that the effects are partially compensatory. That this is not the case will be shown in

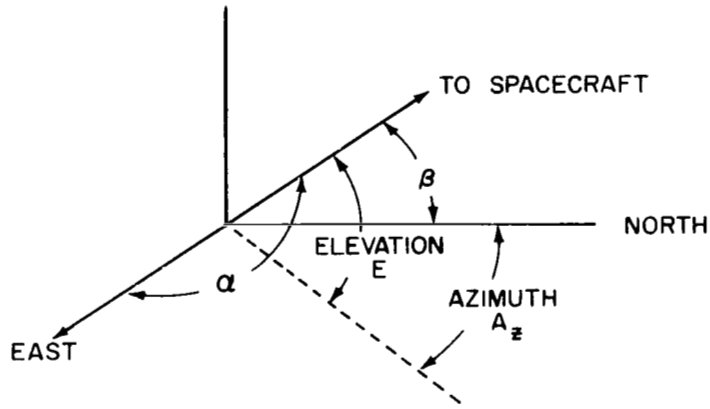

$$\cos E = (\ell^2 + m^2)^{1/2} \qquad \ell \equiv \cos\alpha = \sin AZ \cos E$$

$$\cos AZ = \frac{m}{(\ell^2 + m^2)^{1/2}} \qquad m \equiv \cos\beta = \cos AZ \cos E$$

Figure 4—Definition of Minitrack coordinate system.

section 6.0. However, an intuitive answer may be obtained with reference to Figure 5. By considering a fixed angle of arrival E_o, one can observe what the error ΔE will be for various spacecraft altitudes.

For a given angle of arrival, the ray path is determined; hence, the line-of-sight angle E will always be between the tracking station and a point on the ray trace corresponding to the spacecraft altitude h. As is suggested by Figure 5, the error angle ($\Delta E = E_o - E$) will never be less than the error due to the troposphere alone. The error actually has a maximum when the spacecraft is within the ionosphere; it approaches that due to the troposphere alone as the spacecraft reaches an altitude of several thousand kilometers above the earth's surface.

The correction represented by ΔE_t (Equation 1) is frequency-independent in the range 100 to 20,000 MHz. The correction represented by ΔE_i (Equation 1) varies inversely as the square of frequency. At frequencies greater than 1 GHz and at elevations greater than 5°, the ionosphere accounts for no more than 2% of the total refraction (Reference 6). At 136 MHz, however, the tropospheric and ionospheric refraction effects can be comparable, depending upon spacecraft altitude. At altitudes greater than 100 km and for $E_o > 10°$, the first-order tropospheric elevation correction for tracking spacecraft with a steerable antenna is given by (References 12, 13, and 14)

$$\Delta E_t = N_s(10^{-6}) \cot E_o \,, \tag{2}$$

where ΔE_t and E_o are as defined previously and N_s, the surface refractivity, is a convenient measure of surface index of refraction:

$$n_s = 1 + N_s(10^{-6}) \,. \tag{3}$$

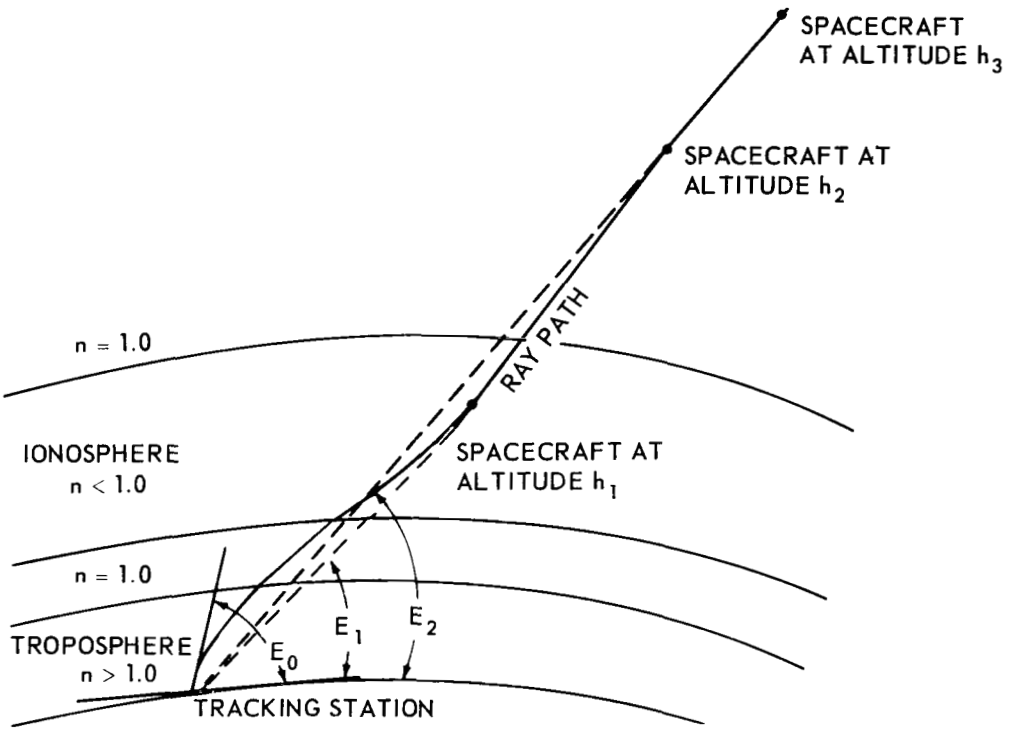

E_0 = ANGLE OF ARRIVAL (FIXED FOR A GIVEN RAY PATH) = CONSTANT
E = LINE-OF-SIGHT ELEVATION (E_1 = LINE-OF-SIGHT ELEVATION TO SPACECRAFT AT h_1 AND E_2 = LINE-OF-SIGHT ELEVATION TO SPACECRAFT AT h_2)
ERROR ANGLE $\equiv \Delta E = E_0 - E$
NOTE THAT $\Delta E_1 > \Delta E_2$ AND $\Delta E \rightarrow$ CONSTANT AS $h \rightarrow \infty$

Figure 5—Increase in elevation angle error due to ionosphere.

The surface refractivity N_s can be computed from

$$N_s = \frac{77.6}{T}\left(P + \frac{4810 e_s \mathrm{RH}}{T}\right), \tag{4}$$

where

T = temperature (degrees Kelvin),

P = total atmospheric pressure (millibars),

RH = relative humidity,

and

e_s = saturation vapor pressure (millibars).

Equations 1 and 2 can also be written in terms of direction cosines. For frequencies above 1 GHz, the ionospheric contribution to ray bending is usually considered negligible and Equation 1 becomes

$$E = E_o - N_s(10^{-6}) \cot E_o \,, \tag{5}$$

or

$$\cos E = \cos \left[E_o - N_s(10^{-6}) \cot E_o\right] \doteq \left[1 + N_s(10^{-6})\right] \cos E_o \,, \tag{6}$$

since, for $E_o > 5°$,

$$N_s(10^{-6}) \cot E_o \ll E_o \,.$$

However, from Figure 4,

$$l = \cos a = \sin AZ \cos E$$

$$m = \cos \beta = \cos AZ \cos E \,.$$

If l_o and m_o represent angle-of-arrival direction cosines and l, m represent "best estimate" of line-of-sight direction cosines, it is seen that:

$$l = \left[1 + N_s(10^{-6})\right] l_o \tag{7}$$

and

$$m = \left[1 + N_s(10^{-6})\right] m_o \,. \tag{8}$$

In summary then, it is seen that a steerable antenna (i.e., monopulse) tracking system, when corrected for first-order tropospheric bending effects, results in the angle-of-arrival direction cosine adjustments indicated by Equations 7 and 8. The next section will show that this tropospheric correction is inherent in the Minitrack direction cosine calculation.

4.0 TROPOSPHERIC ANGLE CORRECTION INHERENT IN INTERFEROMETER MEASUREMENTS

An ideal radio interferometer measurement will be defined as one where the incident signal is planar and operation is within a stable (i.e., time-invariant over measurement period), spherically stratified, exponential troposphere. These conditions are, for all practical purposes, met when radio energy is received from a spacecraft at altitudes in excess of 100 km above the earth's surface and when frequencies in excess of 1 GHz are employed, thus obviating consideration of the ionosphere. At lower frequencies, such as the 136-MHz transmission of Minitrack signals, the ionosphere will also affect the angle measurement. However, this ionospheric effect can be shown to produce a linear addition to elevation angle measurement which will appear as a residual error once the troposphere has been taken into account. The following derivation shows that the ideal interferometer provides a built-in first order correction for the tropospheric effect and that this correction is the same as is normally applied to elevation angle data obtained from steerable antenna trackers (i.e., Equation 2).

4.1 The Basic Minitrack Measurement

As suggested by Figure 6, the basic measurements of an orthogonally intersecting interferometer, such as Minitrack, are the direction cosines l and m. More precisely, however, the measurement is a

phase comparison, which, for each antenna pair, provides a measure of radio path length difference. This is indicated in Figure 6, where S_2-S_1 and S_4-S_3 in actual operation represent radio path length differences rather than geometric differences associated with operation within free space. The object of all elevation angle corrections to radio tracking data is to approximate the geometric line-of-sight elevation angle between tracking stations and spacecraft as closely as possible. This line of sight is indicated by S in Figure 6.

The phase measurement associated with the two interferometer antenna pairs is indicated in Figure 7.

With reference to Figure 6, the direction cosines l_o and m_o of the angles of arrival are given by

$$l_o = \cos \alpha_o = \frac{M_1 \lambda_s}{b} \tag{9}$$

$$m_o = \cos \beta_o = \frac{M_2 \lambda_s}{b}, \tag{10}$$

where M_1 and M_2 are whole and fractional cycles of phase shift measured by the Minitrack system, λ_s is the signal wavelength which would be measured in the refractive media in the immediate vicinity of the interferometer, and b is the baseline separation of each of the interferometer legs.

4.2 Minitrack Angle Computation

The information contained in the raw tracking data is in terms of fractional cycles of phase shift. At GSFC, ambiguities are resolved and the phase counts are converted to direction cosines with baseline

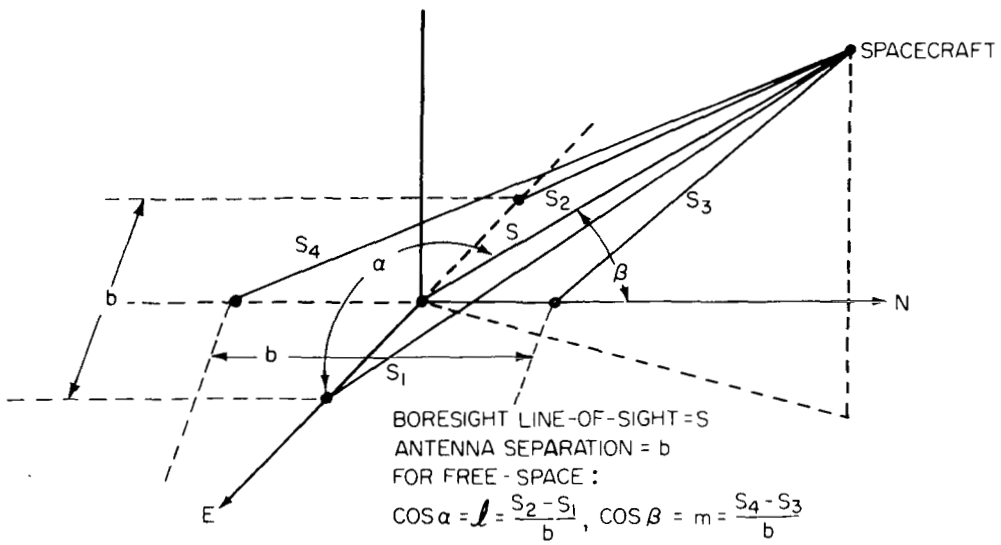

Figure 6—Simplified diagram of Minitrack interferometer spacecraft tracking.

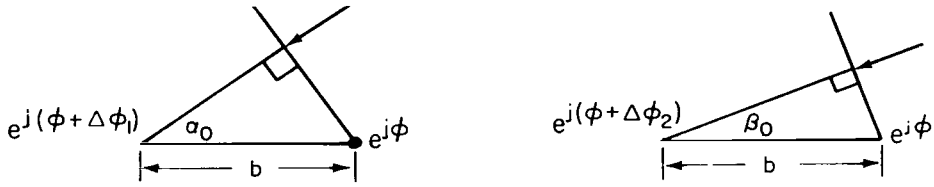

WHERE α_0 AND β_0 ARE RESPECTIVE INTERFEROMETER ANGLES CORRESPONDING TO THE WAVEFRONT ANGLE OF ARRIVAL, E_0

Figure 7—Interferometer phase measurement.

separation in free-space wavelengths λ_o rather than the actual wavelength indicated in Equations 9 and 10 (Reference 15). Thus the angles α' and β' calculated with free-space baseline separation are not a measure of angle of arrival but some "pseudo angle" that is linked to the angle of arrival by the surface index of refraction. That is,

$$\lambda_s = \frac{\lambda_o}{n_s}, \tag{11}$$

and hence

$$\cos a' = l' = n_s \cos a_o = \left[1 + N_s(10^{-6})\right] l_o . \tag{12}$$

Similarly,

$$m' = \left[1 + N_s(10^{-6})\right] m_o , \tag{13}$$

where l' and m' are calculated direction cosines and l_o and m_o are angle of arrival direction cosines. However, Equations 12 and 13 are seen to be exactly the results presented previously by Equations 7 and 8 where a first-order tropospheric correction had been applied to a monopulse (steerable antenna) tracking system. Thus the Minitrack angle calculation has a built-in tropospheric refraction correction which, for $E_o > 10°$, accounts for at least 98% of the tropospheric bending. If no atmospheric corrections are applied to Minitrack data it can be expected that the primary refraction effect of the earth's atmosphere will be linked to the ionosphere.

5.0 OPTICAL AND RADIO REFRACTION DURING MINITRACK CALIBRATION

At present the Minitrack system is calibrated by means of aircraft that carry both optical and radio beacons. The optical beacon is photographed against a star background which permits a precise means for determining the line of sight between station and aircraft (Reference 16).*

The primary purpose of the aircraft flyby is to determine the far-field phase characteristics of the Minitrack antenna array. Since Minitrack antenna spacing corresponding to each of the intersecting

*"Minitrack System Training Manual," (revised September 1958) compiled by the Tracking and Guidance Branch, Project Vanguard, National Aeronautics and Space Administration, Washington, D.C. Part VI, Calibration of Minitrack, by Habib, E. J., Bradford, J. N., Berbert, J. H., Engels, P. D., and Oosterhout, J. D. Can be obtained from the STADAN Technical Reference Control Facility, Code 533, Goddard Space Flight Center, Greenbelt, Maryland.

baselines is on the order of 50 wavelengths, the far field should be probed at slant ranges of approximately 10 km or greater. The aircraft also provide a zero-set phase measurement that accounts for inequalities in cable electrical length between respective antenna arrays and the Minitrack receiver. These cables are filled with moisture-free nitrogen and maintained at an approximate gauge pressure of 5 psi. In addition to the aircraft flyby, internal Minitrack system calibrations are performed to account for electronic equipment phase delays.

5.1 Calibration and Optical Refraction

As indicated in Figure 8, the calibration aircraft is photographed against a star background. The line of sight from the center of the Minitrack's orthogonal pair of interferometers to a given star is then accurately determined since the star field has been well established by astronomers. However, the line of sight to the aircraft differs from the line of sight to the star by a small angle ϵ. This angle, ϵ, must be added to the line-of-sight angle to the star to provide an optical line of sight to the aircraft which is then corrected for radio refraction to permit a calculation of what the interferometer should read at 136 MHz. An expression for ϵ has been rigorously derived in Reference 17. As will be shown in section 5.3 it is also given to a good approximation by

$$\epsilon = \left(n_o - 2 + \frac{\bar{n}}{n_o}\right) \cot \dot{E} ,$$

$$\approx (10^{-6})\bar{N} \cot E \qquad (14)$$

where

E = elevation angle to the star

and

n = surface optical index of refraction.

The term $\bar{n}$, the average optical index of refraction between Minitrack station and aircraft altitudes, is derived from

$$\bar{n} = \frac{1}{H_A - H_s} \int_{H_s}^{H_A} n(h)\, dh = 1 + \bar{N}(10^{-6}) ,$$

where

H_A = altitude of aircraft above sea level,

H_s = altitude of tracking station above sea level,

and

n = optical index of refraction as a function of height,

which for a spherically stratified, exponential troposphere, where $h = H_A - H_s$ [i.e., $n(h) = 1 + N_o(10^{-6})e^{-\gamma h}$], leads to

$$\epsilon \doteq \frac{N_o(10^{-6}) \cot E \left[1 - e^{-\gamma(H_A - H_s)}\right]}{\gamma(H_A - H_s)} , \qquad (15)$$

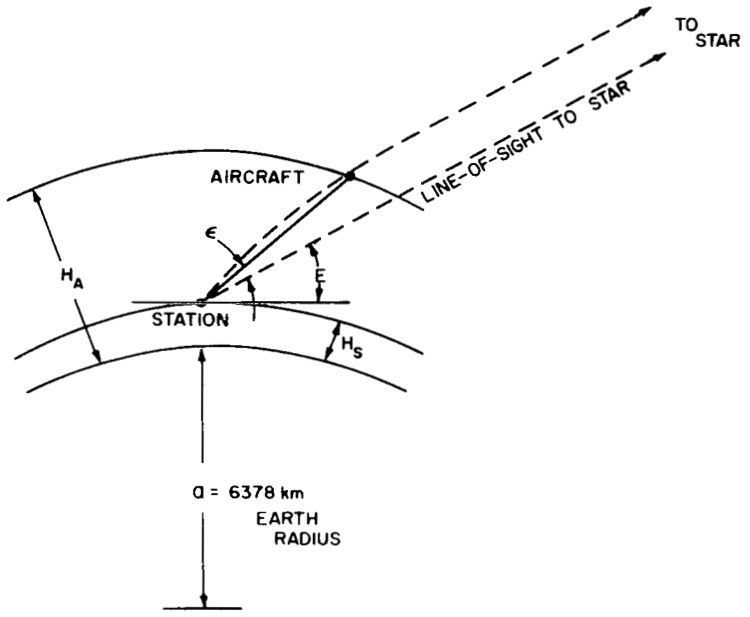

Figure 8—Optical refraction geometry.

where the decay constant γ for the optical index of refraction within the earth's atmosphere is approximately 0.1 km^{-1} (Reference 17).

The validity of the exponential model for purposes of radio refraction correction has been well established (References 7, 12, and 18).

With regard to Equation 15, the optical surface refractivity N_o can be calculated from

$$N_o = \frac{77.6P}{T}, \tag{16}$$

where

P = total atmospheric pressure (millibars)

and

T = air temperature (degrees Kelvin).

The next step is to determine what the Minitrack direction cosine measurements should be, based upon the line-of-sight angle to the aircraft ($E + \epsilon$ of Figure 8). During the calibration, the refracted starlight is made coincident with the flashing light on the aircraft. Let cos α and cos β be the line-of-sight direction cosines to the star as obtained from a star catalog, and let cos α' and cos β' be the desired line-of-sight direction cosines to the aircraft. Then

$$\cos \alpha' = \cos \alpha \left(\frac{\cos \alpha'}{\cos \alpha} \right) \tag{17}$$

and

$$\cos \beta' = \cos \beta \left(\frac{\cos \beta'}{\cos \beta}\right). \tag{18}$$

From previous definitions,

$$\cos a = \sin AZ \cos E ,$$

$$\cos \beta = \cos AZ \cos E ,$$

$$\cos a' = \sin AZ \cos (E + \epsilon) \doteq \sin AZ (\cos E - \epsilon \sin E) , \tag{19}$$

and

$$\cos \beta' = \cos AZ \cos (E + \epsilon) \doteq \cos AZ (\cos E - \epsilon \sin E) . \tag{20}$$

Thus the ratios $\cos a'/\cos a$ and $\cos \beta'/\cos \beta$ (Equations 17 and 18, respectively) are given by

$$\frac{\cos a'}{\cos a} = \frac{\cos \beta'}{\cos \beta} = 1 - \epsilon \tan E = (1 - K) . \tag{21}$$

By combining Equations 15 and 21, the correction factor $(1 - K)$ becomes

$$(1 - K) = \left[1 - \frac{N_o (10^{-6}) \left[1 - e^{-\gamma (H_A - H_s)}\right]}{\gamma (H_A - H_s)}\right], \tag{22}$$

and

$$\cos a' = \cos a(1 - K) \tag{23}$$

$$\cos \beta' = \cos \beta(1 - K) , \tag{24}$$

$\cos a$ and $\cos \beta$ being line-of-sight direction cosines to a star coincident with the flashing light and $\cos a'$ and $\cos \beta'$ line-of-sight direction cosines to the aircraft. (Equation 22 is currently employed in the calibration calculation at the Physical Science Laboratory.)

The next section will show that the expected radio phase meter readings $\Delta\varphi_a$ and $\Delta\varphi_\beta$ are given by

$$\Delta\varphi_a = [b \cos a(1 - K)\bar{n}]\left[\frac{2\pi}{\lambda_o}\right] \tag{25}$$

and

$$\Delta\varphi_\beta = [b \cos \beta(1 - K)\bar{n}]\left[\frac{2\pi}{\lambda_o}\right] , \tag{26}$$

where

b = baseline length,

$\cos a$ and $\cos \beta$ = direction cosines corresponding to line of sight to star occulted by the flashing light,

$(1 - K)$ = correction factor to obtain line of sight to aircraft,

$$\bar{n} = \frac{1}{H_A - H_s} \int_{H_s}^{H_A} n(h)\, dh$$ = average radio index of refraction between tracking station and aircraft altitudes,

and

λ_o = free-space wavelength of received frequency.

5.2 Calibration and Radio Refraction

During the aircraft calibration flyby at a given site, radio phase data are recorded and the difference between the observed phase data and that "expected" is sent to Goddard Space Flight Center as a correction to be applied to subsequent raw Minitrack phase data. During this calibration the expected Minitrack radio phase measurement is based upon the precise line of sight to the aircraft adjusted for prevailing radio refraction conditions. The previous section discussed the conversion of star line of sight to aircraft line of sight. This section will derive the radio refraction correction factor.

During calibration the ionosphere plays no part since the aircraft is necessarily well below the ionosphere's 85-km lower altitude limit. A most important point is that the radio phase readings measured during calibration are compared with precise line-of-sight data altered slightly to take into account the tropospheric radio refraction. The calibration is not a means for later adjusting raw spacecraft tracking data to either angle of arrival or line-of-sight measurements; the calibration accounts for on-site biases associated with the Minitrack antenna system and electronics and does not provide a refraction correction for subsequent raw data recordings.

In order to calculate what the interferometer should read for a given line-of-sight geometry, it is necessary to calculate the electrical path difference corresponding to the geometric path difference $S_2 - S_1$ (Figure 9). It will be shown that, for the aircraft geometry, the corresponding electrical path length is given by $\bar{n}(S_2 - S_1)$, where $\bar{n}$ is the average radio index of refraction between tracking site and aircraft altitudes.

With reference to Figure 9, in the absence of an atmosphere the free-space interferometer phase measurement would be given by

$$\Delta\phi_o = \frac{2\pi(S_2 - S_1)}{\lambda_o}, \tag{27}$$

where

S_1 = geometric distance from the phase center of the antenna at one end of the baseline to the aircraft,

S_2 = geometric distance from the phase center of the antenna at other end of the baseline to the aircraft,

and

λ_o = free space wavelength = c/f_o, c being the speed of light in vacuum and f_o the frequency of the received radio energy.

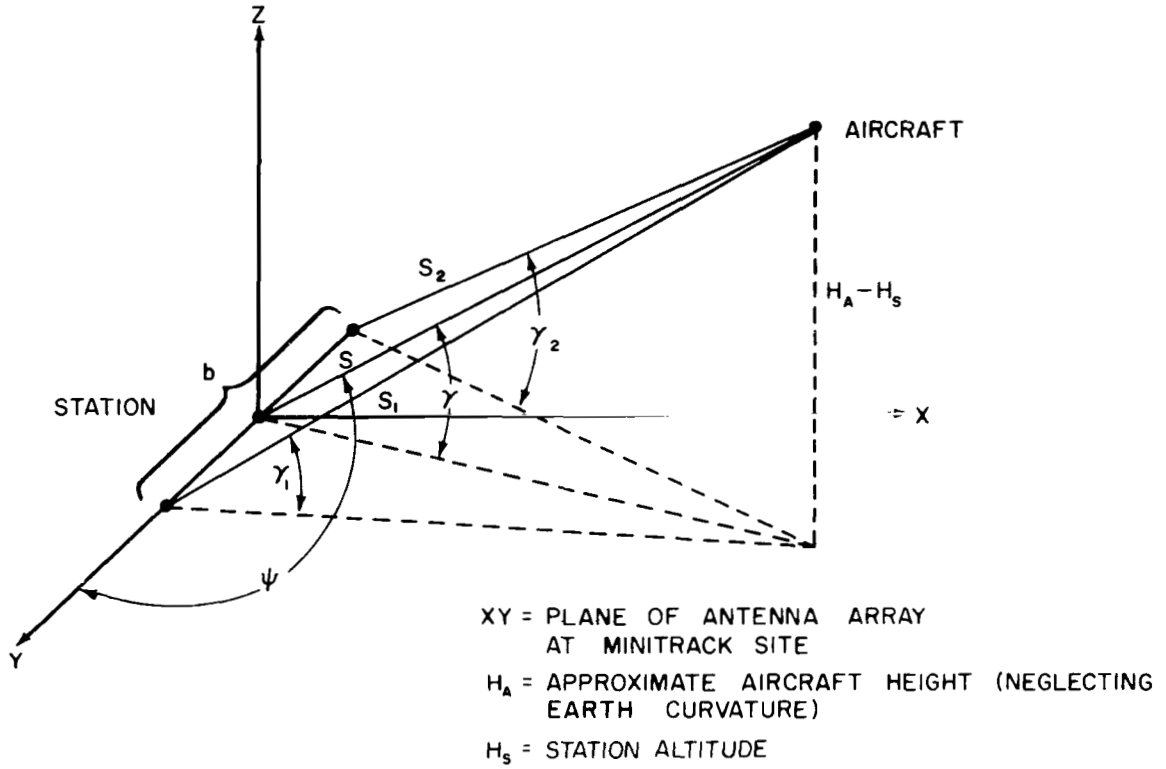

Figure 9—Aircraft calibration geometry.

The frequency f_o will differ from the transmitted frequency by the one-way Doppler shift $f_o(\dot{r}/c)$, where $\dot{r}$ is the radial velocity of the aircraft beacon relative to the station. At 136 MHz, this is entirely negligible relative to the expected uncertainty in the measured surface index of refraction of $\pm 1N$ unit; that is, the ratio of ΔN (± 1) to N_s (~ 300) is always large compared to $\dot{r}/c$. The physics linking surface refractivity to wet- and dry-bulb temperature measurements and statements of expected accuracy is covered in detail in Reference 7.

Again with reference to Figure 9, the actual interferometer phase readings are given by

$$\Delta\varphi = \frac{2\pi}{\lambda_o}\left[\int n(s)\, dS_1 - \int n(s)\, dS_2\right]. \tag{28}$$

As pointed out by Bean and Thayer (Reference 14) of the National Bureau of Standards (NBS), Equation 28 can be integrated assuming flat-earth conditions for elevation angles $E_o > 10°$, slant range $r \ll a_o \sin E_o$ (a_o = earth radius), and baselines of a few hundred meters or less.

These conditions are applicable to the aircraft flyby and hence, again with reference to Figure 9, Equation 28 can be approximated by

$$\Delta\varphi = \frac{2\pi}{\lambda_o}\left(\frac{1}{\sin\gamma_2} - \frac{1}{\sin\gamma_1}\right)\int_{H_s}^{H_A} n(h)\,dh, \tag{29}$$

which neglects ray curvature. Therefore, by the law of sines,

$$\frac{S}{\sin\gamma_1} = \frac{S_1}{\sin\gamma}$$

and

$$\frac{S}{\sin\gamma_2} = \frac{S_2}{\sin\gamma},$$

Equation 29 becomes

$$\Delta\varphi = \frac{2\pi(S_2 - S_1)}{\lambda_o}\left(\frac{1}{H_A - H_s}\right)\int_{H_s}^{H_A} n(h)\,dh = \frac{2\pi(S_2 - S_1)}{\lambda_o}\,\bar{n}\,. \tag{30}$$

With reference to Figure 9, $S_2 - S_1$, at aircraft slant ranges, is given by

$$S_2 - S_1 = b\cos\psi\,.$$

For one Minitrack baseline, $\psi \equiv \alpha'$; for the other orthogonal Minitrack baseline, $\psi \equiv \beta'$. In relation to the star direction cosines, α and β, Equation 30 can be written as

$$\Delta\varphi_\alpha = [b\cos\alpha(1 - K)\bar{n}]\frac{2\pi}{\lambda_o}$$

and (31)

$$\Delta\varphi_\beta = [b\cos\beta(1 - K)\bar{n}]\frac{2\pi}{\lambda_o},$$

where the factor $(1 - K)$ was defined by Equation 22.

In Equation 31, $\Delta\varphi_\alpha$ and $\Delta\varphi_\beta$ represent the expected Minitrack phase readings during the aircraft flyby when the flashing light appears coincident with a star whose line-of-sight direction cosines are $\cos\alpha$ and $\cos\beta$ respectively.

The average radio index $\bar{n}$ is calculated using the NBS exponential profile $n(h) = 1 + N_s(10^{-6})e^{-kh}$. This profile, when integrated and averaged, results in

$$\bar{n} = 1 + \frac{N_s(10^{-6})\left[1 - e^{-k(H_A - H_s)}\right]}{k(H_A - H_s)}\,. \tag{32}$$

The decay factor k is calculated with an empirical relation formulated by NBS based upon a fit to 888 sets of data (Reference 12)

$$k = \log_e \frac{N_s}{N_s + \Delta N},$$

where ΔN represents the change in refractivity in the vertical direction 1 km above the tracking station (Reference 12):

$$\Delta N = -7.32e^{0.005577N_s}. \tag{33}$$

Finally, the surface refractivity is calculated from surface meteorological measurements with the relation

$$N_s = \left(\frac{77.6}{T}\right)\left(P + \frac{4810e_s(\mathrm{RH})}{T}\right), \tag{34}$$

where

n_s = $1 + N_s(10^{-6})$, the surface radio index of refraction,

T = air temperature (°K),

P = total air pressure (millibars),

e_s = saturation vapor pressure (millibars),

and

RH = relative humidity (Reference 19).

The optical surface refractivity N_o, as previously indicated by Equation 16, is Equation 34 without the water vapor term.

Equations 31 through 34 are used by New Mexico State University in their reduction of Minitrack aircraft calibration data for Goddard Space Flight Center.

5.3 Angle of Arrival Correction Equations

As a matter of interest, the foregoing principles can now be applied to derive the flat-earth approximation for the angular difference between elevation angle of arrival and line of sight for both optical and radio refraction. The only difference between the optical and radio cases is that $\bar{n}$ for the radio refraction includes the effect of water vapor within the earth's atmosphere.

For an interferometer such as Minitrack, which has intersecting orthogonal baselines running east-west and north-south, from previous considerations, the phase readings during a spacecraft track are given by

$$\Delta\varphi_a = \frac{2\pi b \cos E}{\lambda_o}\bar{n} \sin AZ$$

and

$$\Delta\varphi_\beta = \frac{2\pi b \cos E}{\lambda_o}\bar{n} \cos AZ. \tag{35}$$

Here, E represents the line-of-sight elevation angle to the source and AZ the azimuth angle. The phase measurement is also represented by the phase delay in terms of the number of wavelengths of delay within the media surrounding the antenna. The effective wavelength within the media in the vicinity of the antenna is λ_o/n_s. In terms of the elevation angle of arrival E_o, the following equations can thus be written:

$$\Delta\varphi_\alpha = \frac{2\pi b \cos E_o}{\lambda_o/n_s} \sin AZ$$

and (36)

$$\Delta\varphi_\beta = \frac{2\pi b \cos E_o}{\lambda_o/n_s} \cos AZ \, .$$

Equations 35 and 36 combined yield

$$\bar{n} \cos E = n_s \cos E_o \, . \tag{37}$$

This equation links elevation angle of arrival E_o to line-of-sight angle E; but $E_o = E + \Delta E$, where ΔE is a small perturbation, and Equation 37 can be expanded to obtain the approximation

$$\Delta E \doteq \left(1 - \frac{\bar{n}}{n_s}\right) \cot E \, . \tag{38}$$

Here ΔE is the elevation angle-of-arrival error due to the atmosphere. This result was also derived by R. H. Paul (Equation 19 of Reference 14) using a somewhat different approach. Equation 38 can also be written in terms of refractivity N since

$$\bar{n} = 1 + \bar{N}(10^{-6})$$

and

$$n_s = 1 + N_s(10^{-6}) \, .$$

In all cases the deviation from unity is 10^{-3} or less; thus, Equation 38 can be written as

$$\Delta E = (N_s - \bar{N}) \cot E(10^{-6}) \, , \tag{39}$$

where, as before, N_s represents the radio surface refractivity varying from 200 to 400, depending upon geographical location and local meteorological conditions, and $\bar{N}$ is the average refractivity between the station altitude and the altitude of the signal source. If the source is a spacecraft, then $\bar{N}$ includes the effect of the ionosphere, where the absolute sign of the refractivity term is negative (Reference 6). Equation 39 thus also indicates how the presence of the ionosphere increases the total ray bending as suggested by Figure 5. If the altitude of the spacecraft increases much above 5000 km, or for all spacecraft operating at 2 GHz or higher such that the ionosphere is no longer a significant influence, $\bar{N}$ tends to zero and Equation 39 reduces to

$$\Delta E \doteq N_s(10^{-6}) \cot E \, ,$$

and, to a first order,

$$\cot E = \cot E_o ,$$

or

$$\Delta E \doteq N_s(10^{-6}) \cot E_o . \tag{40}$$

This result, presented earlier as Equation 2, is the usual tropospheric-bending correction applied to elevation-angle spacecraft tracking data for elevation angles above 10°. The same result is used for optical correction to star-light angle of arrival, except that N_o, the optical surface refractivity, is used instead of N_s, the radio-surface refractivity.

Finally, Equations 38 and 40 can be used to derive Equation 14, presented as the angular difference ϵ between the line of sight to a star coincident with a flashing light on the Minitrack calibration aircraft and the line of sight to the aircraft.

With reference to Figure 8, the angle ϵ is the difference between the total star-light bending $N_o(10^{-6}) \cot E$ and the bending of the flashing-light ray path relative to the line of sight to the aircraft $(1 - \bar{n}/n_o) \cot E$:

$$\epsilon = \left[(n_o - 1) - \left(1 - \frac{\bar{n}}{n_o}\right)\right] \cot E ,$$

or

$$\epsilon = \left(n_o - 2 + \frac{\bar{n}}{n_o}\right) \cot E . \tag{41}$$

Equation 41 was presented as Equation 14 and presents a good approximation of elevation angle distortion for elevation angle E_o greater than 10° and slant ranges to the spacecraft much less than $a_o \sin E_o$, where a_o is the earth radius.

6.0 EFFECT OF IONOSPHERE ON MINITRACK MEASUREMENT

The elevation angle bias present in Minitrack measurements below elevation angles of 45° can largely be attributed to residual error after nominal ionospheric corrections have been applied. Unlike the troposphere, the ionosphere is much less predictable, and, as mentioned previously, ionospheric refraction effects vary inversely as the square of the radio frequency. One of the major sources of ionospheric modeling error has to do with the fact that the radio signal often traverses portions of the ionosphere several thousand kilometers from the tracking site, a situation where the usual, spherically stratified Chapman model does not strictly apply. One means of minimizing the ionospheric refraction error is to use only data where the signal is traversing local night regions. Recent studies, however, indicate ionospheric propagation anomalies peaking at local midnight at the South American Minitrack sites (Santiago, Lima, and Quito) (Reference 20). These equatorial region anomalies appear to predominate in the east-west baseline which, as stated in Reference 20, is consistent with existing theories

of ion plasma density alignment north-to-south along the earth's magnetic field lines. Study of the phenomena and the effect on NASA 136-MHz telemetry, tracking, and command signals is continuing.*†

6.1 The Interferometer Refraction Error Equation

The inherent tropospheric correction to interferometer data was discussed in section 4.0. It was shown that the elevation angle calculation is given by

$$E' = E_o - N_s(10^{-6}) \cot E_o$$

and

$$E' \doteq E_o - N_s(10^{-6}) \cot E \,, \tag{42}$$

for $E_o > 10°$, where,

E_o = elevation angle of arrival,

E' = interferometer calculated angle,

and

E = line-of-sight elevation angle.

It was also shown in section 5.3 (Equation 38) that the line-of-sight elevation angle E is linked to angle of arrival elevation E_o by

$$E \doteq E_o - \left(1 - \frac{\bar{n}}{n_s} \cot E\right) . \tag{43}$$

Thus the total interferometer error is found by combining Equations 42 and 43 to obtain

$$\text{Interferometer Error} = E' - E \doteq -\bar{N}(10^{-6}) \cot E \,, \tag{44}$$

which corresponds to Bean and Thayer's Equation 26 in Reference 14. Equation 44 is a good approximation for $E > 10°$, interferometer baselines of a few hundred meters or less (such as Minitrack), and slant range to spacecraft $r \ll a_o \sin E$, where a_o is the earth radius. Equation 44 is useful in qualitatively describing the effect of the ionosphere on Minitrack data when the spacecraft is within the ionosphere (100 km < altitude < 1000 km). At 136 MHz the contribution to $\bar{N}$ due to the troposphere is negligible compared to the ionospheric contribution. This can be shown as follows. According to Equation 32, for altitudes significantly above the troposphere scale height (~7 km), the tropospheric average refractivity is given by

$$\bar{N}_t = \frac{N_s}{kH} \,, \tag{45}$$

*Golden, T. S., "A Proposal for Measuring the Correlation Distance of Equatorial Ionospheric Disturbances," NASA-GSFC Document X-525-68-302, August 1968.

†Golden, T. S., "Effects of Differential Signal Amplitudes in the Minitrack System," NASA-GSFC Document X-525-68-14, January 1968.

where

H = spacecraft height above the tracking station

and

k = decay factor in exponential model, $1/k = 7$ km.

For $H = 200$ km, $\bar{N}_t \doteq 12$, which is small when compared to the ionospheric contribution. The ionospheric refractivity is given by (Reference 6)

$$N(h) = \frac{-40.3 N_e(h)}{f^2} (10^6), \tag{46}$$

where

N_e = electron density (electrons/meter^3)

and

f = frequency (Hz).

For a daytime peak density at the height of maximum ionization, N_e takes on values of typically 0.5×10^{12} electrons/m^3, and at 136 MHz this corresponds to a maximum ionospheric refractivity of the order of -2000. This value will taper off by a factor of 10 at the lower edge of the ionosphere ($H = 85$ km). However, the average contribution will be significantly greater than the tropospheric contribution $\bar{N}_t = 12$. An interesting observation is that, again by Equation 44, and noting that the average refractivity due to the ionosphere is negative, the ray bending will be in the same direction as that due to the troposphere. With the interferometer, of course, the tropospheric bending is already inherently corrected for by the usual angle calculation discussed in section 4.0.

The flat-earth model (Equation 44) is useful for qualitative ionospheric refraction discussion only when the range of validity includes the constraint $r \ll a_o \sin E$. However, a more satisfactory equation, which includes earth curvature, has been presented by Bean and Thayer, where the interferometer error is given by

$$\text{Interferometer Error} = \left[-10^{-6} \cot E \int_0^H N(h)\, dh\right]\left[\frac{1}{r \sin E} + \frac{1}{a_o \sin^2 E}\right], \tag{47}$$

for $E > 10°$ and $r \gg b (b < 50$ km), where

E = line-of-sight elevation angle,

$N(h)$ = vertical refractivity profile including both troposphere and ionosphere,

r = slant range station to spacecraft,

H = altitude of spacecraft above station,

a_o = earth radius,

and

b = interferometer baseline (b = 120 meters for Minitrack).

For the flat-earth approximation ($r \sin E \doteq H$ and $r \ll a_o \sin E$), Equation 47 reduces to $-\bar{N}(10^{-6})$ cot E, presented previously as Equation 44.

Equation 47 can be derived from Snell's law for a spherically stratified media. The result can also be obtained by ray tracing through the atmosphere (again using Snell's law) to determine the difference between angle of arrival and line of sight. This can then be linked to the interferometer error by subtracting out the first order tropospheric correction of $N_s(10^{-6})$ cot E.

6.2 Minitrack Ionospheric Refraction

This section presents the Minitrack bias error that can be expected if ionospheric effects are neglected. A nominal correction based upon NBS monthly worldwide peak electron density predictions and some mathematical distribution model (such as a Chapman profile) often reduce the error by only 50%. The greatest uncertainty is related to the F_2-layer vertical-sounding (i.e., zero) maximum usable frequency (MUF). The peak electron density, and hence refractivity, is proportional to the square of the F_2 (zero) MUF.

As indicated by Figure 5 and Equation 47, the Minitrack refraction error is separable into tropospheric and ionospheric components. At frequencies such as 136 MHz, where ionospheric bending is appreciable, the tropospheric contribution in Equation 47 is generally negligible if elevation angles above 10° and spacecraft altitudes above 100 km are considered. During aircraft calibration the reverse is true and only the troposphere is a consideration. By ray tracing (Reference 21) through the ionosphere and troposphere separately and then comparing with a trace through ionosphere plus troposphere, one may verify the validity of superposition of bending. The difference between total bending due to the troposphere alone and $N_s(10^{-6})$ cot E_o comprises the tropospheric contribution to the error in Equation 47. The ionospheric-caused elevation error in Equation 47 can be obtained directly from a ray trace through the ionosphere alone.

Table 1 is an example of the Minitrack refraction-error magnitude associated with a track of the 2000-km-altitude geodetic satellite GEOS 1 which was launched on 6 November 1965. It should be emphasized that exact refraction values will vary from site to site and depend upon the time of day as well as time of year. For the table a peak ionospheric density of 0.8×10^{12} electrons/m^3 was assumed for daytime and 10^{11} electrons/m^3 for nighttime.

In Table 1, the term bias refers to that value which must be subtracted from the measured elevation to obtain true elevation. The minus sign on the troposphere bias simply indicates the extent to which the inherent $N_s(10^{-6})$ cot E correction of the interferometer overcompensates for the tropospheric bending. Also, the ionospheric refraction is a maximum for satellites at an altitude of approximately 500 km. For an altitude of 500 km, the ionospheric error values of Table 1 will be increased by approximately 25% at 10°, 50% at 20°, and 70% at 30°. The ionospheric bias tabulated in Table 1 is also plotted in Figure 10. The parameters used to obtain the results of Table 1 and Figure 10 via a ray trace are as follows:

Table 1—Minitrack refraction bias (no corrections applied; satellite altitude = 2000 km).

Elevation angle (deg)	Tropospheric bias (mrad)	Ionospheric bias (mrad)	
		day	night
10	-0.06	2.25	0.30
15	-0.02	1.65	0.20
20	-0.01	1.25	0.15
30	-0.005	0.80	0.10
40	-0.002	0.50	0.05
60	-0.001	0.25	0.02
80	~-0.0005	0.10	0.01

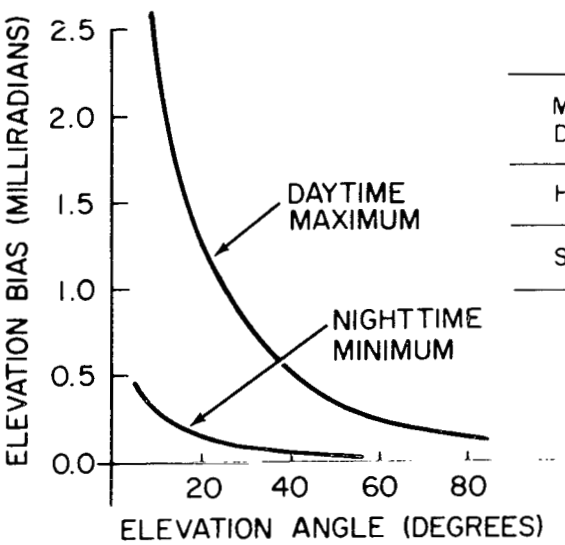

MINITRACK IONOSPHERIC PARAMETERS
(JANUARY 1966 PREDICTION)
REFERENCE 22

	DAY	NIGHT
MAXIMUM ELECTRON DENSITY (ELECTRONS/M^3)	0.8(10^{12})	0.1 (10^{12})
HEIGHT OF MAXIMUM (KM)	300	250
SCALE HEIGHT (KM)	83	66

SATELLITE HEIGHT = 2000 KM

Figure 10—Minitrack elevation angle of arrival bias due to ionosphere if no correction applied.

TROPOSPHERE:

NBS exponential model

$$N(h) = N_s e^{-kh}$$

$$N_s = 350 \quad k = 0.16 \text{ km}^{-1}$$

$$n(h) = 1 + N(h)(10^{-6})$$

$$0 \leqslant h \leqslant 30 \text{ km} \tag{48}$$

IONOSPHERE:

Chapman Model

$$N(h) = \frac{-40.3 N_e(h)}{f^2} 10^6$$

$$f = 136 \text{ MHz}$$

$$n(h) = 1 + N(h)10^{-6} \qquad h > 85 \text{ km}$$

$$N_e(h) = N_m e^{1/2(1-Z-e^{-Z})} \text{ (Reference 23)} \tag{49}$$

N_m = maximum electron density = $0.8(10^{12})$ electron/m^3 representing nominal daytime value,

$$Z = \frac{h - h_m}{H},$$

h_m = 300 km representing a typical daytime height of maximum ionization,

H = scale height = 83 km,

and

h = 2000 km (GEOS 1 altitude).

For a more precise determination of refraction effects, all of the foregoing parameters must be estimated in view of particular station geographical locations, time of year, time of day, phase of sun spot cycle, prevailing meteorological conditions, and so on. It should be pointed out that at present, except for special tracking tests, only Minitrack data above elevation angles of 80° are used for orbit computation.

Figures 11 and 12 are plots of elevation angle residuals (observed elevation minus orbit calculated elevation) when no refraction corrections were applied to a 7-day stretch of GEOS 1 Minitrack data (31 December 1965 to 6 January 1966). It is felt that the trended portion of these curves can be attributed primarily to refraction within the ionosphere.

Finally, a most important point is that the tropospheric error indicated in Table 1 would be the only significant atmospheric refraction bias for an interferometer operating at frequencies above 2 GHz. For such a situation, and for satellites where the slant range approaches the magnitude of the earth radius multiplied by sin E, the interferometer refraction bias is given by the term associated with $1/a_o \sin^2 E$ of Equation 47. This is the expected interferometer refraction bias presented by the National Academy of Sciences (Reference 13) for interferometers with a baseline less than 3 km and operating at high enough frequencies such that the ionosphere is of no concern. The results in Reference 13 check those for the tropospheric refraction presented in Table 1, the latter having been obtained from ray trace considerations.

One might wonder why 136 MHz is used instead of perhaps 2 GHz for the Minitrack frequency to eliminate ionospheric refraction. The primary reason is historical because in 1956, when Minitrack

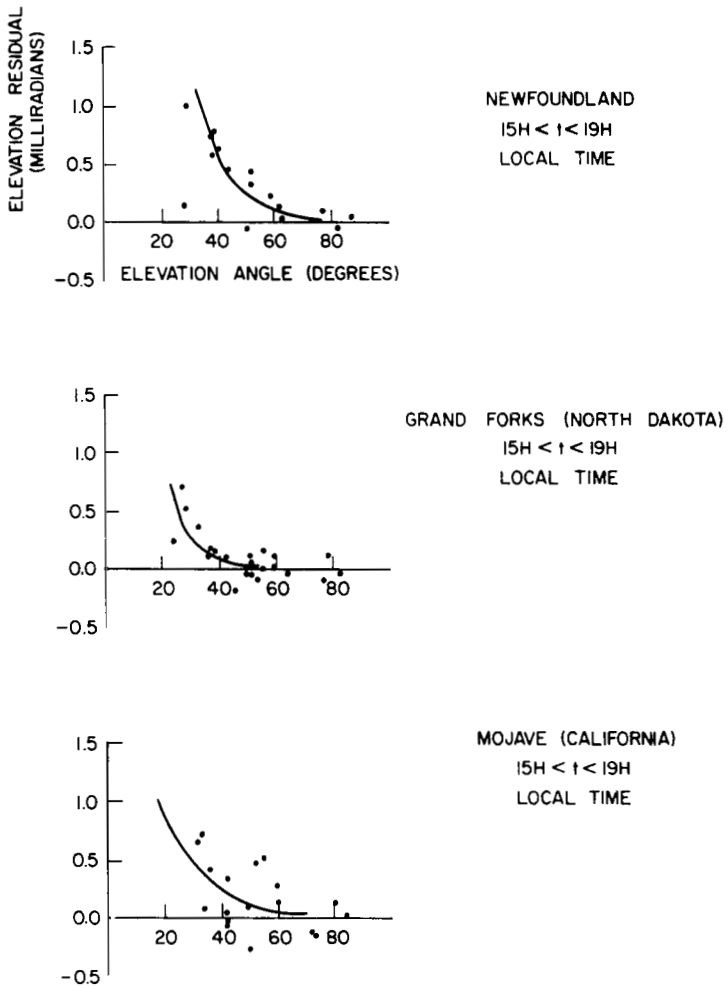

Figure 11–Minitrack elevation angle orbital residuals GEOS 1 (no ionospheric correction).

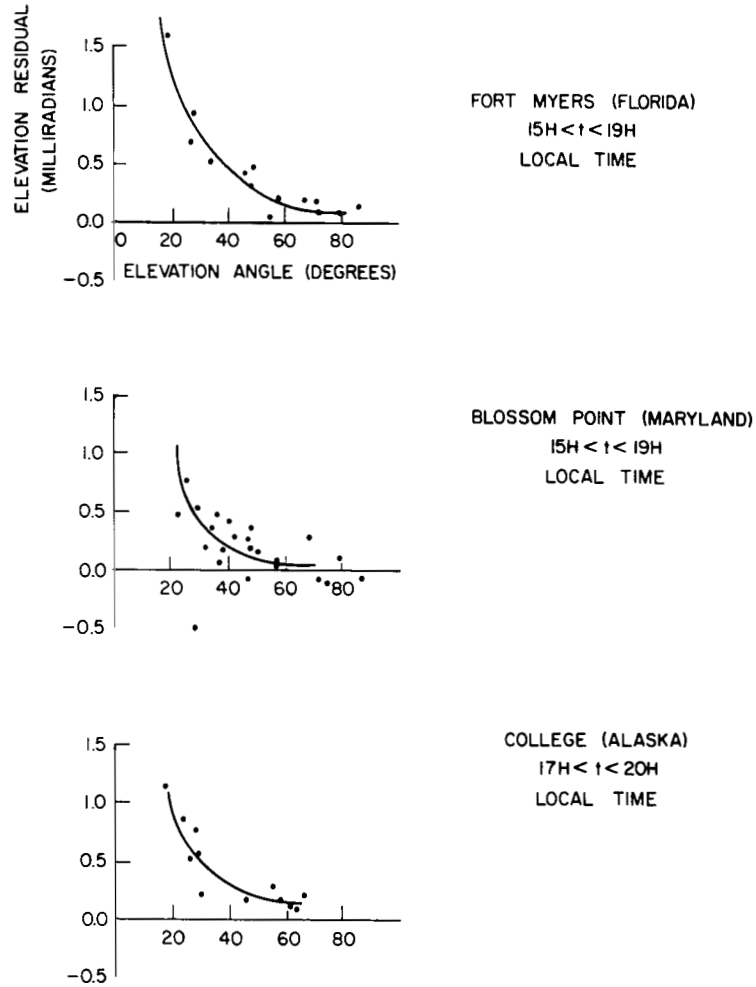

Figure 12–Minitrack elevation angle orbital residuals GEOS 1 (no ionospheric correction).

was first implemented, efficient S-Band spacecraft-qualified hardware was not available. However, the use of 136 MHz still has certain advantages over S-Band, such as ease of signal acquisition and ambiguity resolution. That is, the transfer of radio energy from a spacecraft using a low gain antenna to a given ground-located effective antenna aperture is independent of operating frequency (Reference 24). However, the respective beam and lobe widths vary inversely as the operating frequency. The antenna patterns corresponding to the Minitrack fine resolution array* are given in Figure 13. Note that there are two such arrays for each of two orthogonal baselines. The complete Minitrack antenna layout as given in Reference 15 is shown in Figure 14.

6.3 Ionosphere Model Parameters

The Chapman model presented in section 6.2 as Equation 49 requires three input parameters: the maximum electron density N_m, the height of the maximum h_m, and the scale height H. Of these three, the most critical parameter is the maximum density. The scale height has been formulated in terms of h_m (Reference 25):

$$H = 1.66[30 + 0.2(h_m - 200)] , \tag{50}$$

where H and h_m are in kilometers.

The height of the maximum, if no other information is available, can be taken as h_m = 300 km for daytime and h_m = 250 km for nighttime (Reference 26). The overall refraction is not a critical function of h_m and H.

The following indicates a means for estimating the peak electron density of the ionosphere, utilizing the Institute for Telecommunication Sciences-Environmental Science Services Administration (formerly Central Radio Propagation Laboratory-NBS) monthly publication, *Ionospheric Predictions*, in conjunction with a worldwide, gyro frequency chart.

Ionospheric Predictions presents F_2 (zero) MUF worldwide charts (Reference 22) for 3 months in advance. The charts present monthly mean values in 2-hr increments, since the ionization variations are primarily diurnal during any given month. The "zero" in F_2 (zero) refers to zero ground "skip distance," i.e., vertical incidence ionosphere sounding. It can be shown (see for example, Reference 27) that for vertical incidence the critical frequency (highest frequency signal that will be returned to earth) is a function only of peak electron density and magnitude of the earth's magnetic field in the region of reflection. The direction of the earth's magnetic field does not influence the vertical critical frequency. Because of the presence of the earth's magnetic field, three discrete critical frequencies exist: the ordinary critical frequency (this frequency would be the only critical frequency in the absence of the earth's magnetic field) and two so-called extraordinary critical frequencies. The F_2 (zero) MUF charts are for the highest critical frequency, or the upper extraordinary frequency. This upper frequency results in the more predominant reflection since signals at the lower frequencies encounter appreciable attenuation.

*Lantz, Paul A., and G. R. Thibodeau, "NASA Space-Directed Antennas," NASA-GSFC Document X-525-67-430, September 1967.

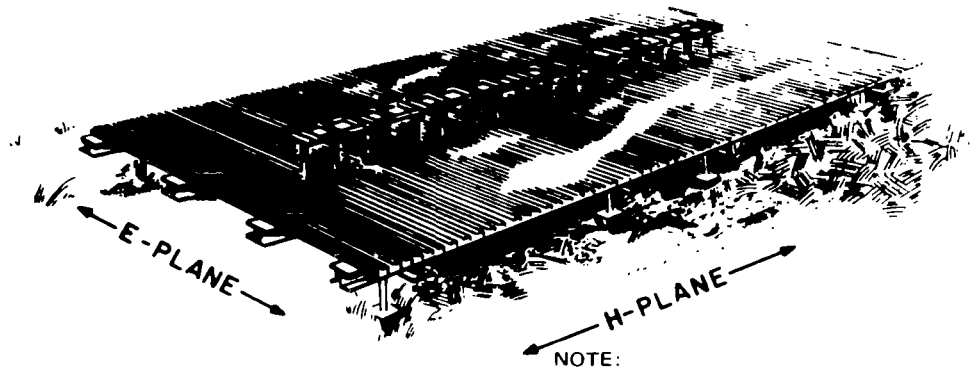

NOTE:
GAIN: 16.3 db ABOVE AN ISOTROPIC SOURCE
2 ARRAYS PER BASELINE

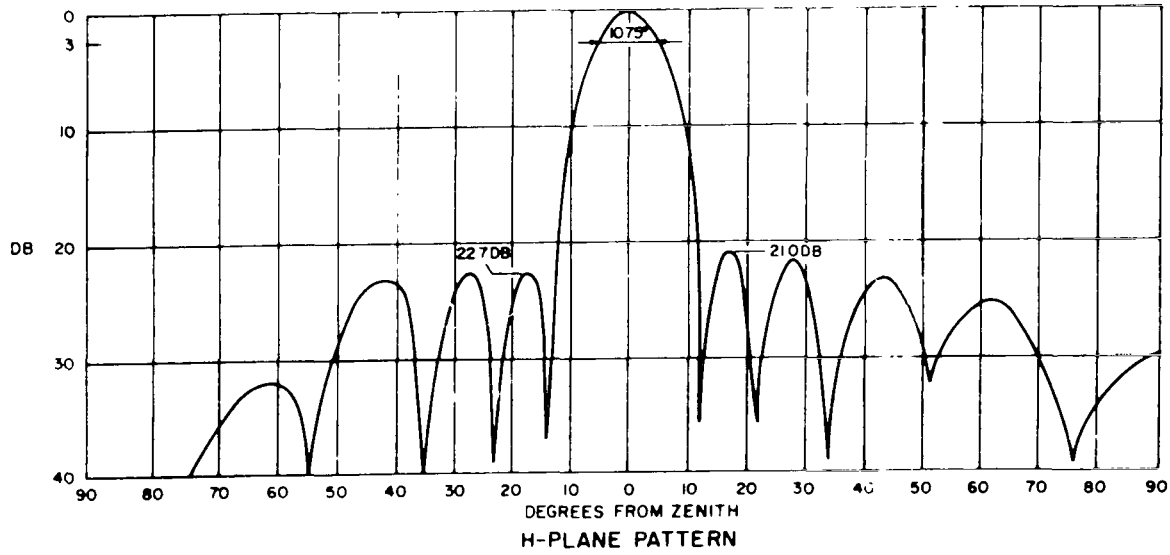

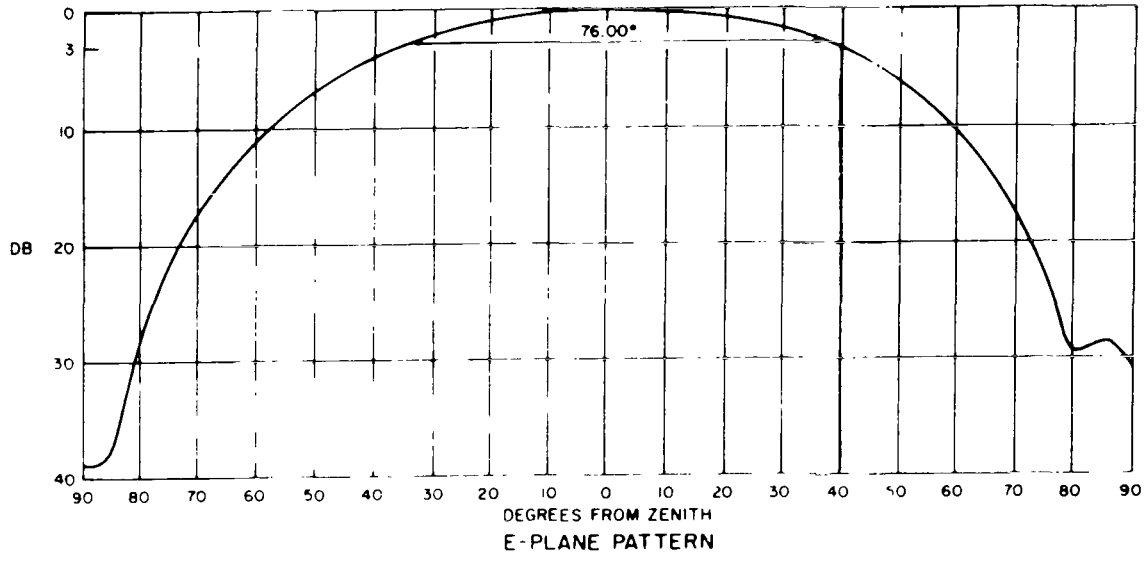

Figure 13—136-MHz Minitrack fine antenna array.

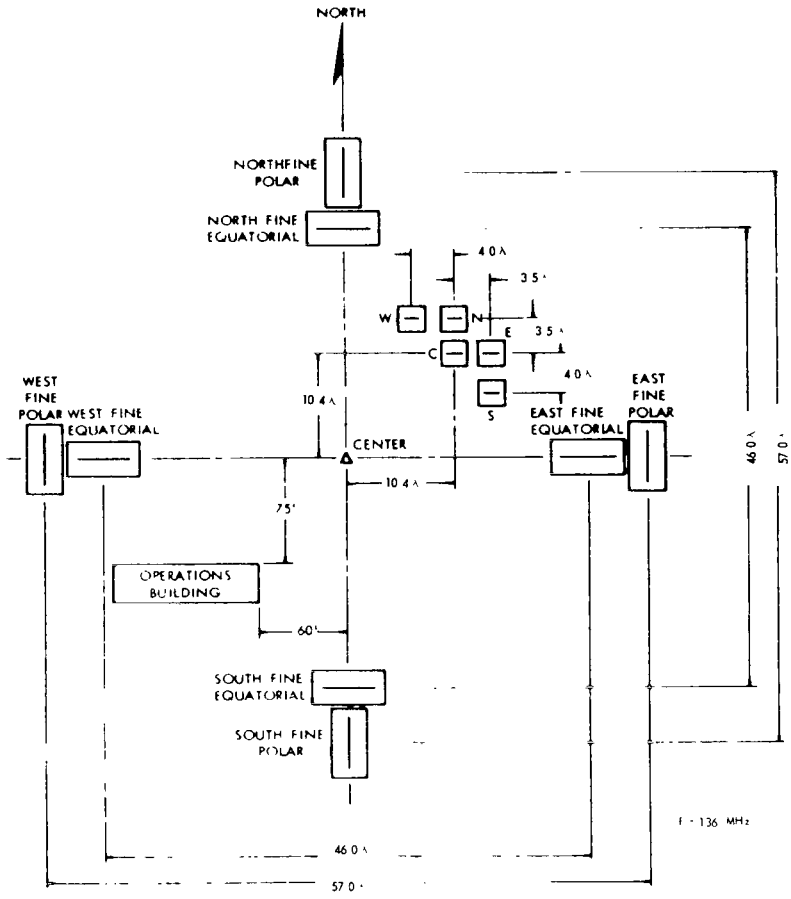

Figure 14--Relative location and function of antennas in a Minitrack antenna field.

The peak electron density is obtained from the ordinary critical frequency as

$$N_e = \frac{f_c^2}{80.6}, \tag{51}$$

where

f_c = ordinary critical frequency (Hz)

and

N_e = peak electron density (electron/m^3).

The F_2 (zero) MUF chart is for the upper extraordinary frequency (e.g., Figure 15) and is related to the ordinary critical frequency as follows:

$$f_{x_1} = \left(\frac{f_h^2}{4} + f_c^2\right)^{1/2} + \frac{f_h}{2}, \tag{52}$$

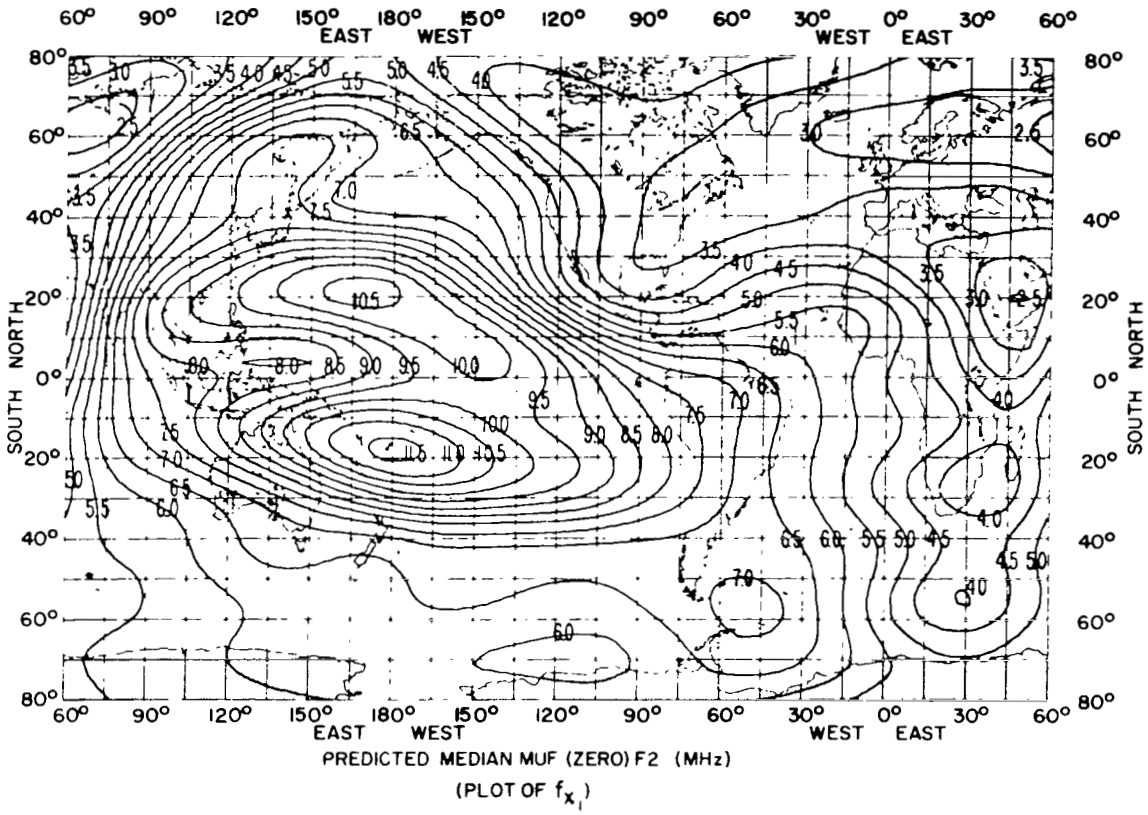

Figure 15—Example of F_2 (zero) MUF prediction (Reference 22).

where

f_{x_1} = upper extraordinary critical frequency as obtained from F_2 (zero) MUF chart,

f_c = ordinary critical frequency required to calculate maximum N_e (Equation 51),

and

f_h = gyro frequency, which couples the effect of the earth's magnetic field into the ionosphere index of refraction (Figure 15).

The last quantity, f_h, is defined (Reference 27) as

$$f_h = \frac{17.6}{2\pi} |\mathbf{B}|$$

where **B** is the earth's magnetic field (Gauss). Since $f_h^2/4 \ll f_c^2$ in most cases,

$$f_{x_1} = f_c + \frac{f_h}{2},$$

or, the ordinary critical frequency is simply

$$f_c = f_{x_1} - \frac{f_h}{2}. \tag{53}$$

The predicted and observed F_2 (zero) MUF values seldom differ by more than 1 or 2 MHz, with the larger differences occurring at the beginning or end of a given month. Unfortunately, the maximum electron density varies as the square of the critical frequency (Equation 51); so for a value of f_c = 5 MHz, under worst case conditions (error of 2 MHz) the electron density could be off by a factor of 2. If the predicted critical frequency is off by only 1 MHz, then the maximum electron density in this case would be correct to within 30%. During mid-month, the F_2 (zero) MUF predicted values are accurate to within 80% to 90%.

The maximum electron density is given by

$$N_M = \frac{[f_{x_1} - (f_h/2)]^2}{80.6}, \tag{54}$$

where

f_{x_1} = frequency for appropriate geographical location, month, and time of day, as obtained from an F_2 (zero) MUF chart such as Figure 15,

f_h = gyro frequency appropriate to a particular tracking site (Figure 16) (note that the gyro frequency is not a function of time),

and

N_M = estimated maximum electron density in the region above a particular tracking station (electrons/m^3).

The maximum electron density N_M calculated by Equation 53 is used in the Chapman model (Equation 49) as a scale factor for the vertical electron density profile. To obtain best results, the profile should be calculated for the region where the radio energy intercepts the region of maximum density. Generally, however, only the region above the tracking site is considered and spherical symmetry is assumed. The error thus introduced depends on satellite altitude and the relative steepness of contours such as given by Figure 15.

7.0 CONCLUSIONS

The atmosphere, for purposes of radiowave propagation, can be separated into two parts: the troposphere (sea level to 30 km) and the ionosphere (85 km to 1000 km). Troposphere refraction effects are frequency independent in the range 100 MHz to 20,000 MHz. Ionospheric refraction is frequency dependent varying inversely as the square of the operating frequency. At 136 MHz ionospheric refraction is significant. The atmosphere influences Minitrack measurements during aircraft calibration and during spacecraft tracking.

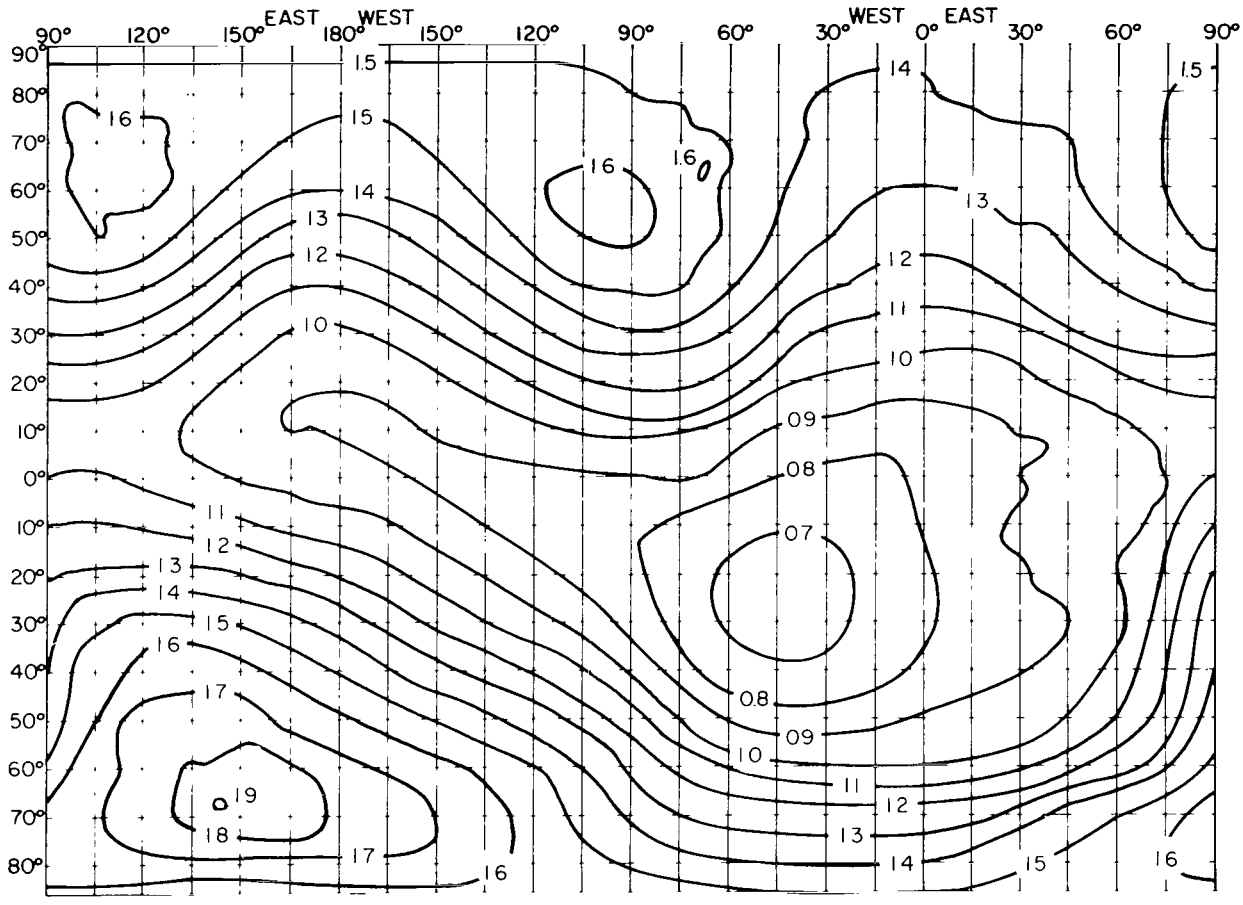

Figure 16—Gyro-frequency map of the world (Reference 28).

AIRCRAFT CALIBRATION

1. Only the troposphere is a consideration for both radio and optical (star background and flashing light) refraction.

2. The NBS exponential atmosphere coupled with flat-earth geometry is satisfactory for modeling aircraft calibration refraction.

3. For this model only the scalar quantity, surface refractivity (optical and radio), is required.

SPACECRAFT TRACKING

1. Only the ionosphere is a consideration since the troposphere is inherently corrected for by the Minitrack calculation.

2. The ionosphere can be modeled using a Chapman-type profile to obtain estimates of ionospheric induced bias.

3. Recent top-side satellite soundings suggest that electron density decays with altitude somewhat less rapidly than predicted by the Chapman model. An exponential decay in electron density above the height of maximum density appears to approximate more closely the true profile.

4. The parameters maximum electron density, height of maximum density, and scale height are required.

5. The extent to which corrections are successful is highly dependent on validity of estimates for maximum electron density.

6. Published prediction for maximum density used at the beginning and end of a given month can be such that as much as 50% of ionosphere residual bias remains after corrections are applied.

ACKNOWLEDGMENT

The cooperation of numerous personnel involved in Minitrack operations, data processing, and orbit computation is hereby gratefully acknowledged. This report was largely guided by the many clarifying discussions held with J.H. Berbert, T.S. Golden, E.J. Lefferts, F.J. Lerch, J.W. Marini, J.D. Oosterhout, W.M. Rice, B. Rosenbaum, F.O. Vonbun, and E.R. Watkins, Jr. at GSFC; H.C. Parker and R.F. Reich at RCA; E. Good at New Mexico State University; and T.S. Englar of Mathematical Sciences Group.

Goddard Space Flight Center
National Aeronautics and Space Administration
Greenbelt, Maryland, February 17, 1970
311-07-21-01-51

REFERENCES

1. Marsh, J. G., Doll, C. E., Sandifer, R. J., and Taylor, W. A., "Intercomparison of the Minitrack and Optical Tracking Networks Using GEOS-I Long Arc Orbital Solutions, Part I," NASA Technical Note D-5337, National Aeronautics and Space Administration, Washington, D.C., December 1967.

2. "Goddard Range and Range Rate System–Design Evaluation Report," General Dynamics R67-042, General Dynamics Electronics Division, San Diego, Calif., December 1967.

3. "Proceedings of the Apollo Unified S-Band Technical Conference," NASA Special Publication 87, National Aeronautics and Space Administration, Washington, D.C., 1965.

4. Barton, D. K., "Radar Systems Analysis," Englewood Cliffs, New Jersey: Prentice-Hall, Inc., 1964.

5. "Applications Technological Satellite Range and Range Rate System–Design Evaluation Report," General Dynamics R65-013, General Dynamics Electronics Division, San Diego, Calif., 1965.

6. Schmid, P. E., "Atmospheric Tracking Errors at S- and C-Band Frequencies," NASA Technical Note D-3470, National Aeronautics and Space Administration, Washington, D.C., August 1966.

7. Bean, B. R., and Dutton, E. J., "Radio Meteorology," National Bureau of Standards Monograph 92, National Bureau of Standards, Gaithersburg, Maryland, March 1966.

8. Martin, C. F., and Vetter, J. R., "Error Sensitivity Function Catalog," NASA Contractor Report 1511, National Aeronautics and Space Administration, Washington, D.C., April 1969.

9. Mengel, J. T., "Tracking the Earth Satellite, and Data Transmission by Radio," *Proc. IRE* June 1956.

10. Schroeder, C. A., Looney, C. H., Jr., and Carpenter, H. E., Jr., "Tracking Orbits of Man-Made Moons," *Electronics* 32(1): 33–37, January 2, 1959.

11. Schmid, P. E., "The Conversion of Fundamental Tracking Data to Metric Form," NASA Technical Memorandum X-63479, National Aeronautics and Space Administration, Washington, D.C., January 1969.

12. Saxton, J. A., ed., "Advances in Radio Research," Vol. 1, New York: Academic Press, Inc., 1964.

13. Barton, D. K., "Interaction Errors Due to Atmospheric Refraction," in "Summary of National Academy of Sciences AD HOC Report on Electromagnetic Propagation," Washington, D.C.: National Academy of Sciences, pp. 285–322, February 1963.

14. Paul, R. H., Thayer, G. D., and Bean, B. R., "A Comparison of Radar and Radio Interferometer Refraction Errors," *IEEE Trans. Aerosp. and Electron. Syst.* 22: 346–350, March 1969.

15. Watkins, E. R., Jr., "Preprocessing of Minitrack Data," NASA Technical Note D-5042, National Aeronautics and Space Administration, Washington, D.C., May 1969.

16. Good, E. W., Berbert, J. H., and Oosterhout, J. D., "Reduction of the Minitrack Astrographic Plates," *Photographic Science and Engineering* 6(6): 324–327, November-December 1962.

17. Vonbun, F. O., "Correction for Atmospheric Refraction at the NASA Minitrack Stations," NASA Technical Note D-1448, National Aeronautics and Space Administration, Washington, D.C., August 1962.

18. Bean, B. R., and Thayer, G. D., "CRPL Exponential Reference Atmosphere," National Bureau of Standards Monograph 4, National Bureau of Standards, Gaithersburg, Maryland, October 1959.

19. Bean, B. R., Horn, J. D., and Ozanich, A. M., Jr., "Climatic Charts and Data of the Radio Refractive Index for the United States and the World, National Bureau of Standards Monograph 22, National Bureau of Standards, Gaithersburg, Maryland, November 1960.

20. Golden, T. S., "Ionospheric Distortion of Minitrack Signals in South America," NASA Technical Memorandum X-63136, National Aeronautics and Space Administration, Washington, D.C., February 1968.

21. Rosenbaum, B., and Snow, N., "A Programmed Mathematical Model to Simulate the Bending of Radio Waves in Atmospheric Propagation," NASA Technical Memorandum X-63651, National Aeronautics and Space Administration, Washington, D.C., May 1968.

22. "Ionospheric Predictions, January 1966," Number 34, Environmental Science Services Administration, Washington, D.C., October 1965.

23. Kelso, J. M., "Radio Ray Propagation in the Ionosphere," New York: McGraw-Hill Book Co., Inc., 1964.

24. Schmid, P. E., "The Feasibility of a Direct Relay of Apollo Spacecraft Data via a Communication Satellite," NASA Technical Note D-4048, National Aeronautics and Space Administration, Washington, D.C., August 1967.

25. Freeman, J. J., "Final Report on Ionospheric Correction to Tracking Parameters," J. J. Freeman Associates Inc., Silver Spring, Maryland, under Contract No. NAS 509782 for Goddard Space Flight Center, November 1965.

26. Berger, W. J., and Ricupito, J. R., "Refraction Correction Studies," Aeronutronic Publication U-954, prepared for U.S. Army Ballistic Missile Agency, Redstone Arsenal, Huntsville, Alabama, under Contract No. DA-04-495-506 ORD-1900, Aeronutronic Division of Philco-Ford, Newport Beach, Calif., July 1960.

27. Bremmer, H., "Terrestrial Radio Waves," Amsterdam: Elsevier Publishing Company, pp. 276–284, 1949.

28. Davies, K., "Ionospheric Radio Propagation," National Bureau of Standards Monograph 80, National Bureau of Standards, Gaithersburg, Maryland, November 1965.

NASA-Langley, 1971 —— 7

NATIONAL AERONAUTICS AND SPACE ADMINISTRATION
WASHINGTON, D. C. 20546

OFFICIAL BUSINESS

FIRST CLASS MAIL

POSTAGE AND FEES PAI
NATIONAL AERONAUTICS
SPACE ADMINISTRATION

"The aeronautical and space activities of the United States shall be conducted so as to contribute . . . to the expansion of human knowledge of phenomena in the atmosphere and space. The Administration shall provide for the widest practicable and appropriate dissemination of information concerning its activities and the results thereof."

— NATIONAL AERONAUTICS AND SPACE ACT OF 1958

NASA SCIENTIFIC AND TECHNICAL PUBLICATIONS

TECHNICAL REPORTS: Scientific and technical information considered important, complete, and a lasting contribution to existing knowledge.

TECHNICAL NOTES: Information less broad in scope but nevertheless of importance as a contribution to existing knowledge.

TECHNICAL MEMORANDUMS: Information receiving limited distribution because of preliminary data, security classification, or other reasons.

CONTRACTOR REPORTS: Scientific and technical information generated under a NASA contract or grant and considered an important contribution to existing knowledge.

TECHNICAL TRANSLATIONS: Information published in a foreign language considered to merit NASA distribution in English.

SPECIAL PUBLICATIONS: Information derived from or of value to NASA activities. Publications include conference proceedings, monographs, data compilations, handbooks, sourcebooks, and special bibliographies.

TECHNOLOGY UTILIZATION PUBLICATIONS: Information on technology used by NASA that may be of particular interest in commercial and other non-aerospace applications. Publications include Tech Briefs, Technology Utilization Reports and Technology Surveys.

Details on the availability of these publications may be obtained from:

SCIENTIFIC AND TECHNICAL INFORMATION OFFICE

NATIONAL AERONAUTICS AND SPACE ADMINISTRATION

Washington, D.C. 20546